A Statistical Representation of Bond Coating Oxidation under Environmental Barrier Coatings

Mackenzie Ridley[1,*], Bruce Pint[1]

[1]*Materials Science and Technology Division, Oak Ridge National Laboratory, Oak Ridge, TN, USA*

**Corresponding Author Email: ridleymj@ornl.gov*

Abstract: Environmental barrier coatings (EBCs) protect SiC based ceramic matrix composites (CMCs) in turbine hot sections from high-temperature volatilization in combustion gases. The formation of a SiO_2 thermally grown oxide (TGO) is expected under the EBC after long term operation. The oxidation resistance of the EBC is understood as a life-limiting factor for the CMC, and this work predicts long term oxidation behavior under EBCs through a simple statistical approach. Specimens were exposed to 1350°C isothermal conditions for 100-hour thermal cycles in flowing steam for up to 1000 hours. The EBC morphology, SiO_2 thickness, and SiO_2 cracking behavior were assessed. Using thousands of SiO_2 thickness measurements across many millimeters of the interface, a realistic representation of the entire thermally grown oxide was captured via a lognormal distribution. The lognormal fit parameters were extrapolated out to 25,000 hours to assess the degree of SiO_2 growth, the spread of SiO_2 thicknesses related to the rough oxidizing interface, and percentages of the intermediate bond coating consumed. Local interfacial defects from the coating deposition process are identified as local failure points for EBC – CMC systems.

Keywords: environmental barrier coating; SiO_2; oxidation; cracking

Introduction

The primary function of environmental barrier coatings (EBCs) is to protect SiC ceramic matrix composite (CMC) turbine hot section components from high-temperature oxidation and volatilization reactions [1, 2]. A metallic Si bond coating is applied between the EBC and the CMC to promote adherence and provide an additional oxidation barrier for the CMC. While EBCs can entirely mitigate volatilization of

a SiO_2 thermally grown oxide (TGO), the formation of a SiO_2 TGO still occurs on the Si bond coating through moisture diffusion from the gas phase through the EBC.

Steam oxidation of Si involves both SiO_2 formation and SiO_2 volatilization, resulting in paralinear oxidation kinetics [1]. With an EBC top coating, only parabolic oxidation kinetics are expected for the Si bond coating. Thus, the TGO growth rate is expected to follow an inverse square root dependence with increasing exposure time. This fundamental oxidant diffusion process is likely what governs component lifetime, as the EBC adhesion strength dramatically decreases as the TGO thickens [3, 4]. The EBC is initially chemically and mechanically bonded to the Si bond coating from the thermal spray process, although the growth of a TGO changes both the bonding layer chemistry and bonding layer thermomechanical properties. Further, the adhesion strength deteriorates from the development of cracks in the TGO throughout thermal cycling. A true parabolic growth rate (i.e. reaction order of 0.5) is not always realized in experiments due to chemical and morphological reasons such as EBC thickness, phase stability, density, splat morphology, interfacial defects, and adhesion quality. Atmospheric plasma spray is known to produce such complex microstructures with a high density of local defects at interfaces and within the deposited coatings [5–9]. Thus, variable TGO growth can be expected locally at the bond coating interface [10–12].

It is typical to take laboratory test specimens and perform cross-section metallography to assess the TGO thickness after a given exposure time and temperature. The number of measurements is normally dependent on the person analyzing data and not always reported in the open literature. A common practice is to present the average (with standard deviation), the median value, or the data range within a 1.5 interquartile range. In all above instances, the outlier measurements (arising from local defects inherent to the APS deposition process) are left out of oxidation rate analyses. Yet, it is imperative to analyze the entire oxidation front, local defects included, to identify future failure points and predict coating lifetimes.

In this work, EBC/Si/SiC coupons were exposed to flowing 90% water vapor/10% air in 100h thermal cycles up to 1000h. The 100h thermal cycle was chosen to be more representative of industrial gas turbines compared to the more commonly performed 1h thermal cycle test for aerospace applications. Specimens were cross-sectioned after each exposure, and a high number of measurements were made across many millimeters of interface to provide statistics on the full EBC performance. The EBC morphology, SiO_2 thickness, and cracking in the SiO_2 scale were all assessed. A simple statistical analysis was performed without fixing the reaction order to 0.5 i.e. parabolic growth, and the oxidation process was predicted for hypothetical exposure times up to 25,000h to support understanding of coating lifetime development.

Methodology

Chemical vapor deposition (CVD) SiC substrate disks were 17 mm in diameter and 2 mm thick. The substrates were grit blasted and coated by atmospheric plasma spray (APS) with a nominally 40 µm thick Si bond coating and 190 µm $Yb_2Si_2O_7$ EBC. SiO_2 loss during APS is common [8], depending on thermal spray parameters, and as such the nominal EBC chemistry was 60% $Yb_2Si_2O_7$ and 40% Yb_2SiO_5 . Specimens were heat treated in a laboratory air box furnace at 1300°C for 4h with a 10°C/min heating and cooling rate prior to testing. This heat treatment was performed to ensure crystallinity and phase stability of the EBC after the plasma spray process[13, 14].

Specimens were hung on SiC rods and placed over an Al_2O_3 sample boat for furnace exposure. Specimens were inserted into the furnace at room temperature, upon which the furnace was heated to 1350°C at 5°C/min. Hot gas was flown over the specimens at 1.5 cm/s, composed of 90% H_2O (g) / 10% laboratory air. A high steam concentration is typically chosen for laboratory scale atmospheric pressure oxidation testing to be more prototypic to the high total pressure and low steam partial pressure environment witnessed by components in the combustion region of gas turbines. Samples were exposed

for 100 h increments, after which the furnace was air cooled, coating integrity was inspected, and sample mass was recorded. A single specimen was removed after specific exposure times ranging from 100 – 1000 h of exposure.

After testing, specimens were mounted in resin, sectioned in half with a low-speed saw, and polished with colloidal SiO_2. Cross-section analysis consisted of backscattered electron (BSE) scanning electron microscopy (SEM) to analyze the EBC morphology changes and SiO_2 TGO growth. Yb_2SiO_5 particle size was measured from BSE SEM images with an image analysis software. TGO thickness was determined using an open source code developed at Oak Ridge National Laboratory[15, 16] which determines the closest distance between the upper and lower TGO boundaries by image greyscale contrast. Specimen edges (~2-4 mm) were not analyzed to ensure that edge artifacts were not included in the data. Channel cracks within the SiO_2 TGO were also counted and SiO_2 thickness at channel cracks were measured manually with ImageJ analysis software. Only cracks that extended at least 75% through the TGO thickness in the 2D image plane were counted.

Results

EBC Morphology Changes during Oxidation Testing

The EBC morphologies are shown in Figure 1 for the initial material before testing and after 1000h of steam furnace exposure. Figure 1 a,c are BSE SEM images, and Figure 1 b,d are binary image segmentations showcasing the monosilicate and disilicate phases. The Yb_2SiO_5 secondary phase microstructure can be seen to undergo immense coarsening over the exposure time of the component. While the splat structure from APS remains visible after 1000h of steam exposure at 1350°C, the nanometer Yb_2SiO_5 particulates are mostly coarsened by 1000h of exposure.

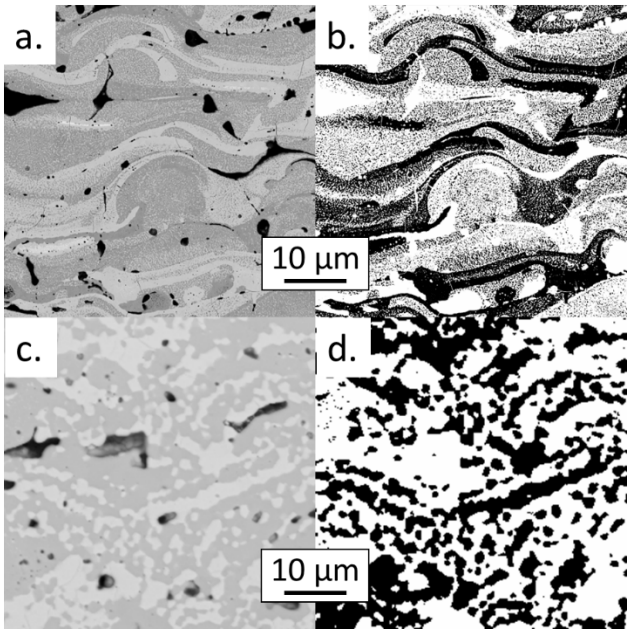

Figure 1. Yb_2SiO_5 particle size from BSE SEM images and with image thresholding, a/b annealed EBC prior to testing, c/d EBC after 1000h at 1350°C. Yb_2SiO_5 phase is black and combined porosity and $Yb_2Si_2O_7$ are white in the threshold images b/d.

Multiple BSE SEM images, summing to 0.2-0.4 mm^2 regions of interest per exposure condition, were analyzed by Yb_2SiO_5 particle area sizes. The average values are shown in Figure 2a; a parabolic fit was witnessed from the coarsening of the monosilicate phase within the EBC. The average values do include both fine particulate and large splat microstructure secondary phases, and as such, error bars provided no quantitative benefit and were not provided in the figure. Instead, Figure 2b was created to visualize the normalized average particle size above and below 10 μm^2. Apart from the pre-test specimen, it is clear that the average size of the large Yb_2SiO_5 splats (>10 μm^2) does not change as a function of exposure time. Rather, the fine Yb_2SiO_5 particulates grow dramatically throughout steam testing.

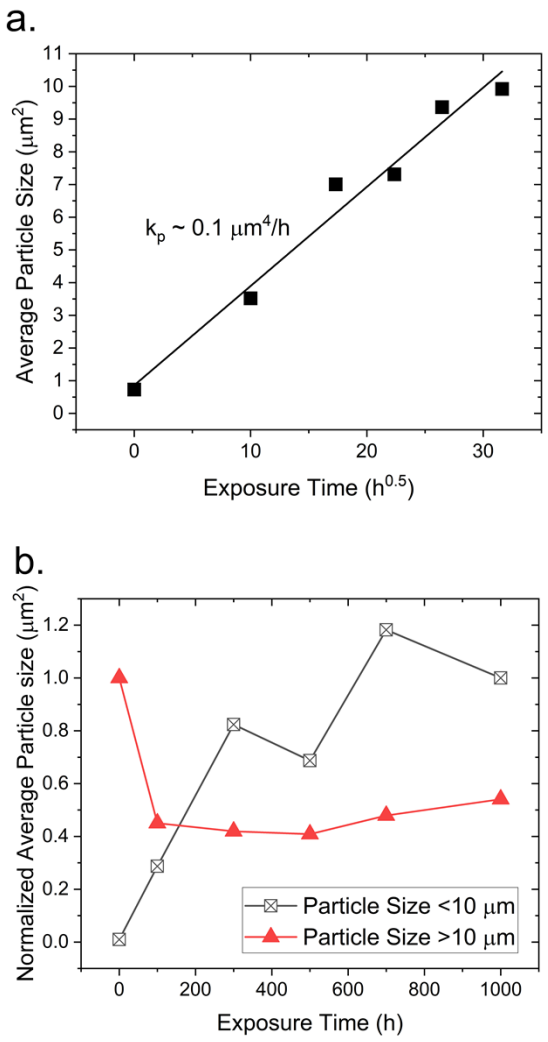

Figure 2. a. Average particle size, b. particle size greater and less than 10 μm.

Statistical Analysis of Oxidation under EBCs

Figure 3 showcases the need for high statistical measurements through analysis of the specimen exposure for 1000h at 1350°C. Cross-sectional images with a total length of ~1850 μm were analyzed, and the total number of equally spaced measurements was varied. The x-axis of Figure 3 corresponds to the measurement spacing (mm/measurement) and the y-axis corresponds to the normalized values of the average, median, upper quartile and lower quartile bounds. As the distance between measurement decreases (i.e. the total number of measurements increases) the average and median SiO_2 thickness values vary only by a few percent difference. A high degree of statistics is likely not necessary for a basic

understanding of SiO_2 thickness under EBCs such as a singular median thickness value. Yet, the upper and lower quartile bounds show a clear deviation from actual values when less measurements are made across the sample interface. The number of measurements needed to fully capture the wide degree of SiO_2 thickness variation along an interface is likely dependent on the deposition process and the resulting interfacial roughness. In this work, a measurement spacing less than 0.2 µm (5 measurements per µm) was used to ensure the SiO_2 thickness variations were fully captured in the analysis.

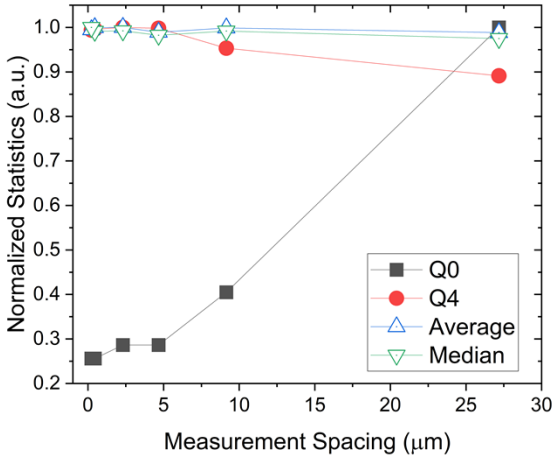

Figure 3. Normalized average, median, minimum (Q0), and maximum (Q4) SiO_2 thicknesses as a function of measurement spacing for the specimen exposed to 1350°C for 1000h. All data were collected on the same set of SEM images, totaling 1850 µm. Data were normalized to the highest value.

Table 1 shows the SiO_2 thickness data collected from the 1350°C oxidation tests. Thousands of measurements over millimeters of cross-sectional length were analyzed from the central regions of each sample after exposure.

Table 1. SiO_2 thickness measurement data.

Exposure Time (h)	Median SiO_2 Thickness (µm)	Average SiO_2 Thickness (µm)	Number of Measurements	Cross-sectional Distance Measured (mm)
100	4.2	5.0±3.6	15,813	2.7
300	5.4	6.3±4.0	11,134	1.8
500	7.0	7.7±4.1	25,480	3.5
700	7.6	8.8±5.0	17,950	4.2
1000	8.8	9.7±4.7	39,824	8.0

Representative BSE SEM images for each sample are shown in Figure 4. As expected, the SiO_2 scale generally increased in thickness with increasing exposure time, yet the scale thickness is nonuniform along the rough and undulating Si bond coating interface. The high degree of statistics encompassed defect regions to ensure that data analysis is representative of the entire sample cross-section. All specimens showed thin SiO_2 streaks along splat boundaries of the Si bond coating which did not grow with time. These SiO_2 regions were a result of the plasma spray deposition process of Si and were not included in measurements of the interface SiO_2 thicknesses.

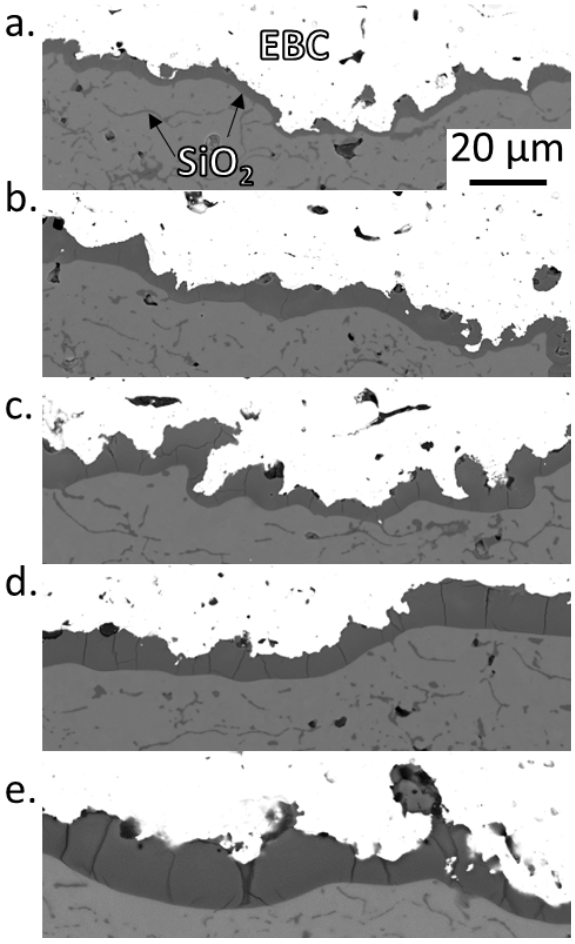

Figure 4. Representative BSE SEM images of each sample showcasing the SiO_2 TGO after a. 100h, b. 300h, c. 500h, d. 700h, and e. 1000h.

Histograms of the SiO_2 thickness data are provided in Figure 5. The baseline material system (i.e. pre-test specimen, heat treated in air to crystallize and equilibrate the EBC) showed a primarily bimodal

SiO_2 distribution, Figure 5a. Local defects provided a maximum initial SiO_2 measurement of ~4 µm, while the average and median thicknesses from the distribution were clearly on the order of hundreds of nm thick. Therefore, the pre-test sample was not included in further analysis. A lognormal distribution was found for all steam exposed samples, Figure 5b.

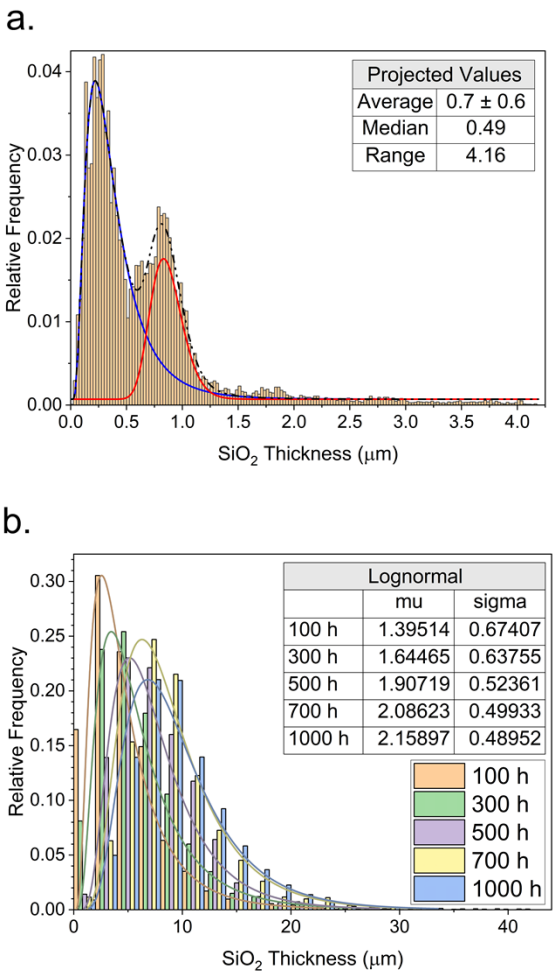

Figure 5. SiO_2 thermally grown oxide thickness distributions a) after equilibration anneal, b) from 100 - 1000 h of total exposure at 1350°C in steam/air mixture.

The lognormal fits from Figure 5b are parameterized by constants through equation 1:

$$f(x) = \frac{1}{x\sqrt{2\pi\sigma^2}}\exp\left(\frac{-1}{2\sigma^2}\left(\ln(x) - \mu\right)^2\right) \quad \text{Eq. 1}$$

where the probability distribution function, f(x), is related to a random variable of interest (x, in this case refers to SiO_2 thickness), the lognormal average (µ) and the lognormal scatter (σ). The change in both µ

and σ as a function of oxidation test time is shown in Figure 6. Both μ and σ followed a linear change on a logarithmic scale as a function of exposure time. A best fit regression was performed to quantify the change in lognormal distribution parameters. The value of μ increased as a function of exposure time, while σ decreased.

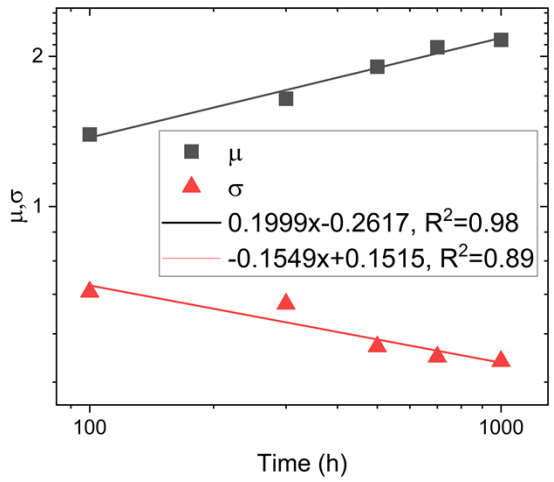

Figure 6. Regression fitting to μ and σ for SiO_2 thickness measurements made up to 1000h of exposure at 1350°C.

Utilizing the best fit equations for μ and σ, extrapolations were made regarding the lognormal distribution for long component lifetimes which are often outside the scope of laboratory research: 2,500h, 5,000h, 15,000h, and 25,000h. Figure 7a shows the projected SiO_2 thickness distributions for the longer time scales. It is expected that the average SiO_2 thickness value increases with increasing hypothetical exposure time, yet a more insightful finding is that the TGO thickness variation in measurement data also increases with exposure in a quantifiable manner.

Average SiO_2 thickness data for the experimental and predicted time scales are presented in Figure 7b on a log-log plot. The black dashed line represents the best fit to the experimental data, assuming a standard 2nd order reaction, where a parabolic oxidation rate of 0.1044 μm^2/h was calculated. The red dashed line was calculated from the fit of the entire experimental and predicted TGO thickness datasets up to 25,000h. A direct calculation of the reaction order from the 100 – 25,000h data was ~0.537,

quite similar to the theoretical slope of 0.5 for parabolic kinetics [17]. The best fit for the experimental and predicted datasets was 0.0915 $\mu m^{1.863}/h$. The statistical reaction rate shows a slightly improved fit to the data, yet both presented rates are within the error for the average scale thicknesses of all exposure times. It should be noted that an assumption of a zero point was used in calculating the reaction rates for both cases due to the more complex initial distribution associated with the crystallization anneal prior to steam testing.

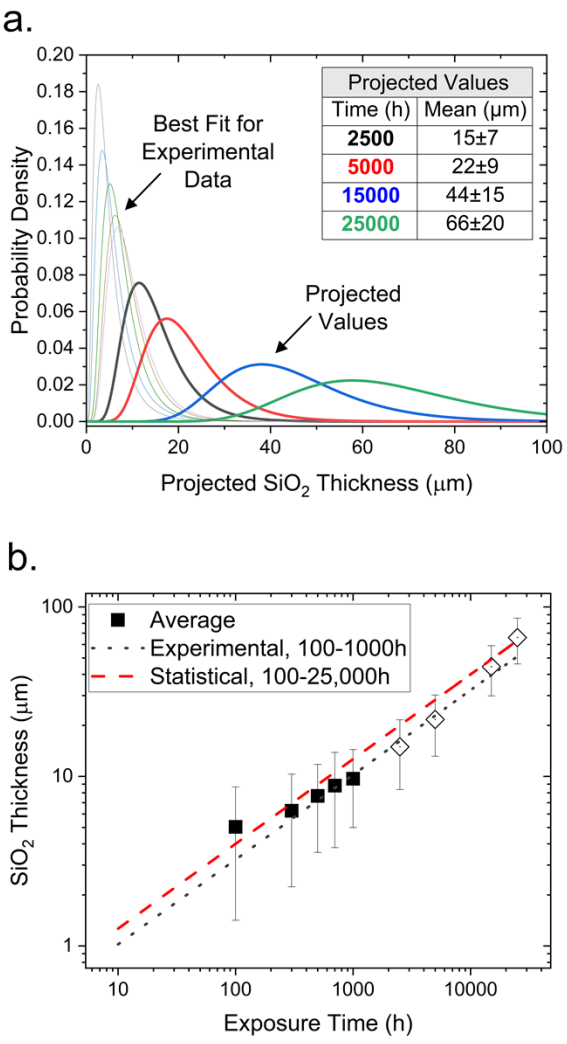

Figure 7. a. Projected SiO_2 thickness lognormal distributions, b. Experimental (0.1044 $\mu m^2/h$) and statistical prediction (0.0915 $\mu m^{1.863}/h$) of average SiO_2 thickness up to 25,000 h exposure at 1350°C.

Quantification of the lognormal distribution can also allow for understanding of EBC failure. Since there is no accepted critical TGO thickness yet for EBC spallation – as this information is dependent on the

EBC properties, test conditions, and specimen geometry – the assumption that the EBC/CMC system will fail once the Si is consumed was applied here. The Pilling-Bedworth ratio of Si is 2.15, suggesting that full consumption of a 40 μm average thickness Si layer would result in an average SiO_2 TGO thickness of 86 μm. It is assumed that an 86 μm TGO would be unrealistic for the current EBC system, and instead a 40 μm SiO_2 thickness is chosen as an upper limit for oxidation prior to EBC spallation. The percentage of TGO measurements greater than 40 microns is shown in Figure 8a. Red triangles indicate experimental percentages, while black squares represent the calculated percentages from the lognormal distributions. No measurements were made where the scale thickness was greater than 40 μm for the 100 and 300h oxidation exposures at 1350°C.

While some measurements were greater than 40 μm for the 500, 700, and 1000h test samples, the measurements associated with those points were due to large scale defects in the material and not indicative of full Si consumption. For example, Figure 8b shows the defect present within the 500h exposure sample TGO analysis dataset. While the SiO_2 scale thickness is locally greater than 40 microns, this was due to a fully oxidized Si splat that appeared to not have been properly adhered to the Si bond coating. A clear increase in predicted bond coating consumption is witnessed at and above 2,500h, where ~94% of the bond coating would be assumed to be fully consumed by 25,000h of exposure at 1350°C.

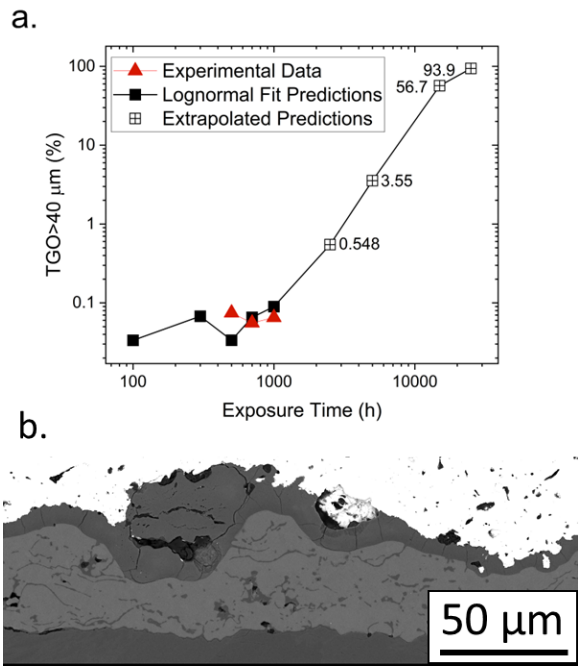

Figure 8. a. Prediction of SiO_2 thickness greater than 40 µm within TGO, measured and predicted from lognormal distribution parameters, b. BSE SEM image of a TGO defect region from the 500h exposure at 1350°C.

Cracking Behavior of SiO_2 TGOs

Crystalline SiO_2 TGOs are known to crack due to a combination of growth, thermal, and phase change stresses during high-temperature exposures. Visualization of regularly spaced channel cracks were shown in Figure 4 and visualization of crack networking in thick TGO regions were shown in Figure 8b. Of primary concern is the cristobalite SiO_2 displacive phase change at 250°C [18–20], which induces a 5% volume change and can weaken the interface through cracking. The thermal properties, such as thermal expansion, can also vary greatly between the alpha and beta cristobalite phases, resulting in a certain magnitude of thermal stress upon cycling[21, 22].

Table 2 shows the number of channel cracks counted and the total distance analyzed for crack counting. All high-resolution SEM images used for analysis were summarized in Figure 9a to provide average crack spacings with standard deviations as a function of exposure time.

Table 2. Analysis of TGO cracking as a function of exposure time at 1350°C.

Exposure Time (h)	Number of channel cracks measured	Distance Analyzed (mm)	Cracks/mm
100	139	0.74	188
300	121	1.1	110
500	215	1.2	179
700	152	1.4	109
1000	238	2.8	85

The average crack spacing generally increased as a function of exposure time at 1350°C with 100h thermal cycles. Statistical differences were found particularly between the 100h and 1000h exposure samples. An increase in the crack spacing implies that stress relief could be occurring at elevated temperatures, where SiO_2 creep may be high enough to seal cracks. High-temperature creep data of cristobalite SiO_2 is not available for validation of the authors' interpretation, although intermediate temperature creep data on quartz SiO_2 has been measured [23] and such data implies that creep may play a significant role in high-temperature cristobalite stress relaxation. Due to the unknown mechanism causing the decreased crack density as a function of exposure time and due to the large error with the limited data collected, a critical TGO thickness for coating spallation could not be determined and additional testing is needed for such identification.

The TGO thickness at each crack was also measured and compared to the total average TGO measurement set, Figure 9b. Excellent agreement was found between both datasets, showcasing that channel cracks form at average thickness locations. High fidelity statistics on the TGO thickness may not be needed for determining a reasonable average scale thickness but are still required for accurate fitting to a lognormal distribution as described previously.

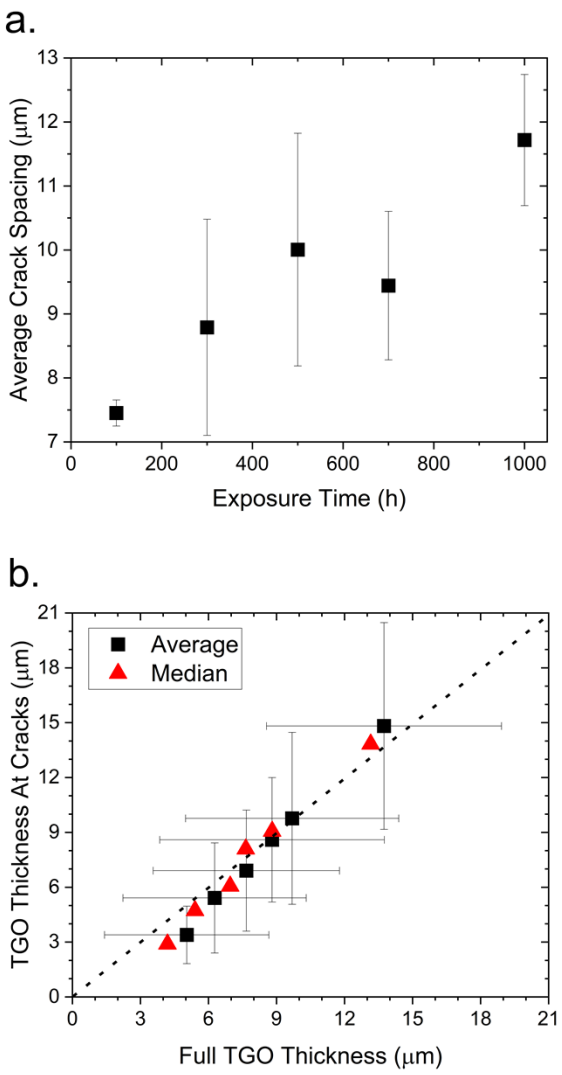

Figure 9. a. Average crack spacing and b. ratio of SiO_2 thickness under cracks to average SiO_2 thickness as a function of exposure time. Bars for each datapoint represent the standard deviation.

Discussion

EBCs are prone to morphology changes at elevated temperatures, even throughout relatively short exposure times under 1000h. In particular, the coarsening behavior of the Yb_2SiO_5 secondary phase can be expected to change moisture diffusion pathways and potentially impact chemical processes such as bond coating oxidation or molten deposit reaction and infiltration kinetics. The changes in grain structure for the $Yb_2Si_2O_7$ primary phase of the EBC was not quantified in this work, although it is expected

that small grains will coarsen at comparable rates to that of the monosilicate phase. Such data can be expected to support multi-scale model development for lifetime prediction of EBCs.

The witnessed trends with lognormal parameters μ and σ provide a basis for understanding the scale growth distribution across a variable roughness interface and support lifetime prediction modeling with enhanced insights compared to more typical kinetic analysis methods discussed in the introduction. While the plasma spray process relies on mechanical and some chemical interaction between layers for coating adherence, the surface preparation procedure and thermal spray parameters can be tailored to minimize the degree of local defects at the interface. For example, Harder et al. showed that EBC bond strength increased with increasing interfacial roughness [3]. Yet, considerations should be made regarding optimization between enhanced roughness for adhesion and minimized roughness for TGO thickness uniformity. Such changes should impact the shape function for the lognormal distribution and as such impact predicted coating lifetimes.

The presented lognormal fit trends allowed for prediction of EBC spallation times through identification of full local consumption of the Si bond coating. A singular kinetic rate only provides average scale thickness, which is expected to be less conservative than consideration of the entire range of scale thicknesses found within a given sample. A perhaps more realistic utilization of the lognormal distributions would be identification of a critical SiO_2 thickness for adhesion failure of the EBC, although such data is coating dependent and not often available in the literature, as TGO measurements under spalled coatings are not reliable. Transitions to linear oxidation kinetics have been reported immediately prior to coating failure[4], likely due to stress evolution within the TGO as a function of scale growth and thermal cycling. Extrapolations of the current data are thus only reliable up the transition point in kinetic behavior leading up to EBC spallation. While the utilization of a lognormal distribution function for TGO growth variations under EBCs is promising for 2- and 3-dimensional modelling and lifetime development of EBC/CMC

systems, additional work is first required to fully understand the TGO cracking behaviors throughout thermal cycling.

Once the bond coating is fully consumed locally, the ceramic component will itself undergo oxidation and accelerated oxidation will occur laterally along the bond coating interfaces. The predicted percentage of localized TGO thickness and subsequent bond coating consumption, shown in Figure 7a and Figure 8a, can be used to estimate the failure time of the EBC. From the predictions, full bond coating consumption in local regions can be expected as early as 2,500 - 5000 h of exposure. Mital et al. suggest that EBC delamination can occur upon reaching an average SiO_2 thickness of 20 – 30 μm [24], which is in general agreement with the statistical predictions shown in this work. Local defects such as those proposed above are likely failure points for coated systems in service, and concepts for nondestructive evaluation of coating and bond coating integrities are needed for health assessment during use. The relationships between TGO channel cracking, crack networking in the TGO, and EBC delamination at the TGO interface should be further studied. Continued efforts must be placed on quantification of stress evolution from the bond coating oxidation process to be able to translate performance metrics between various coating chemistries and morphologies.

Crack spacing analysis as a function of exposure time showed that cracks are spaced further apart with increased scale thickness. The original hypothesis was that crack spacing will decrease with increasing TGO thickness, as the thicker scale will experience a higher degree of stress from particularly phase change and thermal stresses. Crack healing from further oxidation relies on cation species diffusing outward during oxidation[25], yet oxidation of Si is governed by oxidant diffusion inward to the unreacted interface and as such healing of SiO_2 cracks would not be driven by further oxidation. While the present results initially appear counterintuitive, the 100h exposure cycles may provide enough time for creep relaxation of the SiO_2 scale so that crack closure can occur. The authors are aware of the many nuances that underpin segmentation crack measurements, in particular sample preparation effects on artificial TGO crack

development. Yet, it is assumed that sample preparation would be more detrimental to larger, fragile TGOs, and thus more cracks would be induced in specimens with thicker scales. That is not seen experimentally in this work. Given the limited comparative data on SiO_2 crack densities available, and the lacking creep data for cristobalite, this analysis should be repeated for further investigation. A comparative study should also investigate crack behavior with shorter thermal cycles to assess the impacts of creep relaxation time on crack density and spacing.

Conclusions

Yb silicate EBC systems were exposed to 100h cycles in a flowing steam/air mixture at 1350°C to assess bond coating oxidation behavior up to 1000h of total exposure. A statistical prediction of SiO_2 growth was formulated based on the lognormal distribution of scale thicknesses along the bond coating interface, which showed general agreement with the expected parabolic kinetic behavior typically utilized for Si oxidation. The lognormal distribution trends allowed for prediction of thickness variations as a function of time and allow for prediction of thickness-dependent phenomena such as full consumption of the Si bond coating in local interface regions. SiO_2 cracking was measured and the average crack spacing was found to increase as a function of exposure time, implying creep relation of SiO_2 at elevated temperatures during the 100h thermal cycles.

Acknowledgements

The authors would like to thank J. Horenburg, G. Garner, and J. Wade from ORNL for support with testing and metallography. The authors would also like to thank B. Lamm, T. Aguirre, and R. Golden for technical review. This work was funded by the Advanced Turbine Program, Office of Fossil Energy and Carbon Management, Department of Energy.

References

1. Opila EJ. Oxidation and Volatilization of Silica Formers in Water Vapor. *J Am Ceram Soc*. 2003;86(8):1238–1248. https://doi.org/10.1111/j.1151-2916.2003.tb03459.x
2. Lee KN, Fox DS, Eldridge JI, *et al.* Upper Temperature Limit of Environmental Barrier Coatings Based on Mullite and BSAS. *J Am Ceram Soc*. 2003;86(8):1299–1306. https://doi.org/10.1111/j.1151-2916.2003.tb03466.x
3. Harder BJ, Presby MJ, Salem JA, Arnold SM, Mital SK. Environmental Barrier Coating Oxidation and Adhesion Strength. *J Eng Gas Turbines Power*. 2021;143(3):031004. https://doi.org/10.1115/1.4049414
4. Kane K, Garcia E, Lance M, Parker C, Sampath S, Pint B. Accelerated oxidation during 1350°C cycling of ytterbium silicate environmental barrier coatings. *J Am Ceram Soc*. 2021;105(4):2754–2763. https://doi.org/10.1111/jace.18231
5. Herman H. Plasma-sprayed Coatings. *Sci Am*. 1988;259(3):112–117.
6. Vaßen R, Bakan E, Sebold D, Sohn YJ. Correlation of Process Conditions, Porosity Levels and Crystallinity in Atmospherically Plasma Sprayed $Yb_2Si_2O_7$ Environmental Barrier Coatings. *J Compos Sci*. 2021;5(8):198. https://doi.org/10.3390/jcs5080198
7. Bakan E, Sohn YJ, Vaßen R. Metastable to stable phase transformation in atmospheric plasma sprayed Yb-silicate coating during post-heat treatment. *Scr Mater*. 2023;225:115169. https://doi.org/10.1016/j.scriptamat.2022.115169
8. Ridley M, Garcia E, Kane K, Sampath S, Pint B. Environmental barrier coatings on enhanced roughness SiC: Effect of plasma spraying conditions on properties and performance. *J Eur Ceram Soc*. 2023;43(14):6473–6481. https://doi.org/10.1016/j.jeurceramsoc.2023.06.049
9. Garcia E, Sampath S. Phase and properties evolution of plasma sprayed rare earth silicate coatings. *Ceram Int*. 2024;50(13, Part A):23157–23165. https://doi.org/10.1016/j.ceramint.2024.04.039

10. Lee KN. $Yb_2Si_2O_7$ Environmental barrier coatings with reduced bond coat oxidation rates via chemical modifications for long life. *J Am Ceram Soc*. 2019;102(3):1507–1521. https://doi.org/10.1111/jace.15978
11. Bakan E, Vaßen R. Oxidation kinetics of atmospheric plasma sprayed environmental barrier coatings. *J Eur Ceram Soc*. 2022;42(12):5122–5128. https://doi.org/10.1016/j.jeurceramsoc.2022.05.003
12. Ridley M, Kane K, Lance M, *et al.* Steam oxidation and microstructural evolution of rare earth silicate environmental barrier coatings. *J Am Ceram Soc*. 2023;106(1):613–620. https://doi.org/10.1111/jace.18769
13. Garcia E, Garces HF, Turcer LR, Bale H, Padture NP, Sampath S. Crystallization behavior of air-plasma-sprayed ytterbium-silicate-based environmental barrier coatings. *J Eur Ceram Soc*. 2021;41(6):3696–3705. https://doi.org/10.1016/j.jeurceramsoc.2020.12.051
14. Bakan E, Vaßen R. Crack healing mechanisms in atmospheric plasma sprayed Yb-silicate coatings during post-process heat treatment. *J Eur Ceram Soc*. 2023. https://doi.org/10.1016/j.jeurceramsoc.2023.02.005
15. Stack P. SOFIA: Size of Oxidation Feature from Image Analysis. https://github.com/TriplePointCat/SOFIA-CV. 2021.
16. Su YF, Stack PIM, Stephens CJ, *et al.* Quantifying High Temperature Corrosion. Houston, TX: NACE CORROSION. OnePetro; 2021:NACE C2021-16805.
17. Wagner C. Theoretical Analysis of the Diffusion Processes Determining the Oxidation Rate of Alloys. *J Electrochem Soc*. 1952;99(10):369. https://doi.org/10.1149/1.2779605
18. Leadbetter AJ, Wright AF. The α—β transition in the cristobalite phases of SiO_2 and $AlPO_4$ I. X-ray studies. *Philos Mag J Theor Exp Appl Phys*. 1976;33(1):105–112. https://doi.org/10.1080/14786437608221095

19. Lance MJ, Ridley MJ, Kane KA, Pint BA. Raman spectroscopic characterization of SiO_2 phase transformation and Si substrate stress relevant to EBC performance. *J Am Ceram Soc*. 2023;106(10):6205–6210. https://doi.org/10.1111/jace.19190
20. Aguirre T, Lin L, Ridley M, Kane K, Pint B. Finite Element Modeling of the Phase Change in Thermally-Grown SiO_2 in SiC Systems for Gas Turbines. *JOM - J Miner Met Mater Soc*. 2024. https://doi.org/10.1007/s11837-024-06507-4
21. Peacor DB. High-temperature single-crystal study of the cristobalite inversion. *Z Für Krist - Cryst Mater*. 1973;138(1–6):274–298. https://doi.org/10.1524/zkri.1973.138.jg.274
22. Swainson IP, Dove MT. On the thermal expansion of β-cristobalite. *Phys Chem Miner*. 1995;22(1). https://doi.org/10.1007/BF00202681
23. Kirby SH. The effects of the α-β phase transformation on the creep properties of hydrolytically-weakened synthetic quartz. *Geophys Res Lett*. 1977;4(3):97–100. https://doi.org/10.1029/GL004i003p00097
24. Mital SK, Ricks TM, Arnold SM, Harder BJ. Modeling of the Influence of Thermally Grown Oxide (TGO) Layers on the Driving Forces in Environmental Barrier Coating Systems. NASA/TM-20210014094. 2021;26.
25. Schütze M. The healing behavior of protective oxide scales on heat-resistant steels after cracking under tensile strain. *Oxid Met*. 1986;25(5):409–421. https://doi.org/10.1007/BF01072918